Supporting Information

DeStefano et al. 10.1073/pnas.1216412110

SI Materials and Methods

Histological and Morphometric Analysis of X-linked hypertrichosis (XLH) Skin Biopsies. Whole-skin biopsies from the affected, carrier, and control individuals were embedded in optimal cutting temperature (OCT) compound, and a microtome cryostat was used to create 12-μm-thick hair follicle sections. Sections were stained with hematoxylin and eosin, permanently mounted with Permount (Thermo Fischer Scientific), and imaged using an HRc AxioCam fitted onto an Axioplan2 fluorescence microscope (Carl Zeiss). For morphometric analysis, the length-measuring tool in the AxioVision (release 4.8.2) program was used to calculate the distance between two points for each of the indicated hair follicle components; the widest distance for each structure was used, and the average value was taken using two to four measurements per section (with three to six sections per slide). Hair follicles were analyzed from one control and two affected individuals, where each skin biopsy contained two hair follicles, both of which were analyzed.

Isolation and Culture of Human Keratinocytes and Fibroblasts from Whole-Skin Biopsies. Keratinocytes and fibroblasts were grown from control, carrier, and affected skin biopsies using the following protocol: skin biopsies were collected in 10% (vol/vol) FBS in Dulbecco's Modified Eagle Medium (DMEM), washed with 5 mL PBS, and then chopped into small pieces that were transferred to 5 mL Dispase (5 mg/mL) overnight at 4 °C. Epidermis and dermis were separated with a scalpel, and the epidermis was placed into 5 mL 0.25% trypsin–EDTA at 37 °C for 30 min and then into 20 mL 10% (vol/vol) FBS in DMEM. Cells were collected by centrifugation at 1,000 × *g* for 7 min and resuspended in epidermal keratinocyte growth media, defined with supplements (CnT-07; CELLnTECH). Fibroblasts were isolated by digesting the dermis in 10 mL 0.3% collagenase for 4 h at 37 °C. Cells were collected by centrifugation at 1,200 × *g* for 10 min, washed in 30 mL fibroblast culture medium [10% (vol/vol) FBS in DMEM] twice, and then resuspended in fibroblast culture medium.

Whole-Genome Sequencing. DNA was prepared for sequencing according to the Illumina DNA sample preparation kit protocol. Initially, the DNA was randomly fragmented by nebulization followed by end repair, addition of a single A base, adaptor ligation, and gel electrophoresis to isolate 300-bp fragments followed by PCR amplification. Next, the size-selected libraries were used for cluster generation on the flow cell. All prepared flow cells were run on the Illumina HiSeq using the paired-end module: the paired-end reads were each 100 bp long. DNA was aligned to the reference genome (National Center for Biotechnology Information Build 36 Ensembl release 50) using the BWA software (version 0.4.9) (1). Picard was used to remove potential PCR duplicates via the rmdup command. SAMtools (version 0.1.5c) was used for variant identification, using the pileup command with the –c option and default settings (2). The variants were then filtered using a SAMtools variation filter with the default settings but removing the filter for a maximum allowed coverage per variant by setting it to 10 million. All variants were screened for quality by keeping only those with a consensus score and quality score of at least 20 [50 for insertions/deletions (INDELs)] and that had at least three reads supporting the variant. Heterozygous INDELs were also excluded if the ratio of variant reads to reference reads was less than 0.2. The average coverage for this sample was 44.4×. Large deletions and duplications were identified with the Estimation by Read Depth with SNVs software. Structural variants including insertions and translocations were identified using SV-Finder, software developed in the Duke Center for Human Genome Variation that uses multiple alignment-based approaches with an emphasis on split-read and pair-end.

The genomewide identification of functional gene variants was facilitated by SequenceVariantAnalyzer (3).

Amplification of Genomic DNA. The reaction conditions were as follows: 95 °C for 5 min, 94 °C for 30 s, 55 °C for 40 s, and 68 °C for 1.5 min, where 35 cycles were run with a final extension time of 10 min at 68 °C. The primers used for the control reaction were (F) TGGCATTACAAGAGTTAGCTTCTGA and (R) AATGCTTTGTAGTGGCTTTGTTTCC, producing an amplicon of 1,911 bp (4); the primers used for the centromeric breakpoint were (F) TGGCATTACAAGAGTTAGCTTCTGA and (R) CCTCCAGGGTGACTAAATTTG, producing an amplicon of 1,813 bp; and the primers used for the telomeric breakpoint were (F) AACTAGAAGGCCATTGGCTG and (R) AATGCTTTGTAGTGGCTTTGTTTCC, producing an amplicon of 609 bp.

Quantitative RT-PCR Analysis. The primers used in these assays were as follows: human Fibroblast Growth Factor 13 (*hFGF13*) (core)—(F) CAGCCGACAAGGCTACCAC and (R) GTTCCGAGGTGTACAAGTATCC; human MCF2 cell line derived transforming sequence (*hMCF2*)—(F) GCAGCAGGAACTTTTGACAG and (R) GCTGGTGTGTTCCAATTCAG; human SRY related HMG box 3 gene (*hSOX3*)—(F) GTTGGGACGCCTTGTTTAGC and (R) TAGCGCGAAGAAATATCAAACAG (4): human Coagulation Factor IX (*hF9*)—(F) GCATTCTGTGGAGGCTCTATC and (R) GCTGCATTGTAGTTGTGGTG; human ATPase, class VI, type IIC (*hATP11C*)—(F) GGACATTTCTGGCTGCCTTTG and (R) CCAGAATCGGGTATCCAAG; *hK14*—(F) GGGATCTTCCAGTGGGATCT and (R) GCAGTCATCCAGAGATGTGACC; and *hGAPDH*—(F) ATGGACACGCTCCCCTGACT and (R) GAAAGGTGGGAGCCTCAGTC. *hFGF13* isoform-specific PCR was performed using the following primers: *FGF13-001* (1S)—(F) CGAGAAATCCAACGCCTGC (5) and (R) CACCACTCGCAGACCCACAG; *FGF13-002* (1U)—(F) GTTAAGGAAGTCGTATTCAGAGC (5) and (R) CACCACTCGCAGACCCACAG; *FGF13-203* (1V)—(F) GATGCTTCTAAGGAGCCTCAG and (R) CACCACTCGCAGACCCACAG; *FGF13-202* (1Y)—(F) ACAGAGCCGGAAGAGCCTCAG and (R) CACCACTCGCAGACCCACAG; and *FGF13-201, -3* (1V+1Y)—(F) GATGCTTCTAAGGTTCTGGAT and (R) CACCACTCGCAGACCCACAG.

Expression was normalized to the GAPDH housekeeping gene and compared with the control samples. For each assay, cDNA was used from three controls, three carriers, and three affected individuals unless indicated otherwise. For expression analysis of microRNAs, human–miR-504 and human–miR-505, the following miScript primer assays (Qiagen) were used: Hs_miR-504_1, Hs_miR-505_1, and Hs_RNU6-2_1 miScript (miScript PCR Control). Images were generated using GraphPad Prism.

Whole-Mount and Section in Situ Hybridization. For mouse section in situ hybridization, dorsal skin isolated from Swiss Webster mice at indicated time points was harvested and embedded in OCT, where a microtome cryostat was used to generate 10-μm sections. For human studies, 12-μm hair follicle sections were used. The sense and antisense riboprobes were constructed using in vitro

transcription and the Digoxigenin (DIG)-labeling system (Roche). The following primers were used and recognize the core region of the *FGF13* sequence: mouse Fgf13 (*mFgf13*)—(F) TCAAACCAAGCTGTATTTGGC and (R) CTTTCAGTGGTTTGGGCAGAA; and *hFGF13*—(F) AGCCTCAGCTTAAGGGTATAG and (R) CAAGAACACTGTTACCTTGAGC.

Immunofluorescence Staining on Skin Biopsies. Sections were fixed with acetone at −20 °C for 10 min, washed three times in 1× PBS, and then blocked in 1.5% (vol/vol) fish gelatin/1% (vol/vol) BSA in 1× PBS at room temperature for 1 h. The rabbit anti-FGF13 antibody recognizing the C terminus of the protein was generously provided by Geoffrey Pitt (Duke University, Durham, NC) and was used at a concentration of 1:400 in 1.5% (vol/vol) fish gelatin/1% (vol/vol) BSA in 1× PBS. The rat anti-mouse CD200 antibody (1:100) (BD Pharmingen), guinea pig anti-human K75 (1:1,000) (a gift from Lutz Langbein, German Cancer Research Center, Heidelberg) and rabbit anti-human K14 (1:1,000) (Covance) were diluted in 1.5% (vol/vol) fish gelatin/1% (vol/vol) BSA in 1× PBS. The anti-rabbit, -rat, and -guinea pig IgG isotype (Santa Cruz Biotechnologies) antibodies were used as primary controls at the same concentrations as the respective primary antibodies listed above. Following PBS washes, the Alexa Fluor 488 donkey anti-rabbit IgG (Molecular Probes, Invitrogen), Alexa Fluor 594 donkey anti-rat IgG (Molecular Probes, Invitrogen), and Alexa Fluor 594 goat anti-guinea pig IgG (Molecular Probes, Invitrogen) secondary antibodies were added to the cryosections at a concentration of 1:800 in 1× PBS. Sections were mounted in VECTASHIELD mounting medium with DAPI (Vector Laboratories) and imaged using a LSM 5 laser-scanning Axio Observer Z1 confocal microscope (Carl Zeiss). For human studies, Z-stack images were taken at 10× and 20× magnifications using identical settings and consistent Z-stack intervals between slides. For mouse studies, images were taken at a 20× magnification.

Statistical Analysis. A Student *t* test (two-tailed) was used to determine statistical significance in quantitative RT-PCR assays with a significance level (α) of 0.05. Three biological replicates were used in each analysis (unless indicated otherwise), and values represent the average of three independent experiments for the three biological replicates. Error bars represent the SEM.

Assessment of X-Inactivation Skewing in Female Carriers. The human androgen receptor assay (HUMARA) was performed to determine skewing of X inactivation as previously described (6). Genomic DNA from five female carriers was used for amplification of a differentially methylated CpG dinucleotide site near a polymorphic region in exon 1 of the *Androgen Receptor* (*AR*) gene, and PCR products were digested with the HpaII (methylation-sensitive) and RsaI (cocutter, methylation-insensitive) restriction enzymes to distinguish between methylated and nonmethylated alleles. *X-chromosome-inactivation* skewing percentage was determined using the method described in ref. 6.

RNA Sequencing in Whole Skin. RNA sequencing (RNA-seq) was performed on whole skin from one control and one affected individual. Preparation of the cDNA library for sequencing was performed using the TruSeq kit (Illumina). In brief, 100 ng total RNA extracted from affected and control skin biopsies was purified (using polyA capture to select for mRNAs), fragmented, and converted into single-stranded cDNA using random hexamer priming. Next, the second strand was generated and double-stranded cDNA was purified using bead capture. End repair was then performed to create blunt ends, followed by adenylation of the 3′ ends (to prevent intramolecular ligation), ligation of indexing adaptors to the ends of the double-stranded cDNA, and enrichment of DNA fragments containing adaptor molecules using PCR. The resulting cDNA library was then sent to the genomics core facility at The Rockefeller University to be sequenced on the Illumina HiSeq. 2000 machine using single-end reads of ∼50 bp, with an overall sequencing depth of ∼15 million reads per sample. Reads were mapped to the human reference genome (National Center for Biotechnology Information build 37.2) using TopHat, an algorithm designed to align reads from an RNA-Seq to a reference genome based on existing transcript annotation and inferred new splice sites (7). To estimate the relative abundance of genes and splice isoforms, the data were then analyzed using Cufflinks, a program that contains algorithms that estimate transcript abundance while accounting for alternative splicing (8). Fragments per kilobase of exon per million fragments mapped were normalized to the upper quartile. Differential expression of isoforms was tested using Cuffdiff, a program that uses the Cufflinks transcript quantification engine to determine transcript levels in more than one condition.

***In Silico* Prediction Analysis of miR-504 Target Genes.** miR-504 target genes were determined using a comprehensive database, miRWalk (9), which provides information on predicted, validated, and published microRNA target genes. We applied filters to select target genes with a minimum seed sequence of seven nucleotides, the longest transcript of a given gene, and a *P* value of 0.05 or less, which represents the strength of the prediction through a Poisson distribution. Furthermore, target genes that appeared in three or more of the following prediction programs were selected: TargetScan, miRanda, miRDB, PICTAR5, miRWalk, RNA22, and DIANA-mT.

1. Li H, Durbin R (2009) Fast and accurate short read alignment with Burrows-Wheeler transform. *Bioinformatics* 25(14):1754–1760.
2. Li H, et al.; 1000 Genome Project Data Processing Subgroup (2009) The Sequence Alignment/Map format and SAMtools. *Bioinformatics* 25(16):2078–2079.
3. Ge D, et al. (2011) SVA: Software for annotating and visualizing sequenced human genomes. *Bioinformatics* 27(14):1998–2000.
4. Zhu H, et al. (2011) X-linked congenital hypertrichosis syndrome is associated with interchromosomal insertions mediated by a human-specific palindrome near SOX3. *Am J Hum Genet* 88(6):819–826.
5. Wang C, et al. (2011) Fibroblast growth factor homologous factor 13 regulates Na+ channels and conduction velocity in murine hearts. *Circ Res* 109(7):775–782.
6. Warburton D, et al. (2009) Skewed X chromosome inactivation and trisomic spontaneous abortion: No association. *Am J Hum Genet* 85(2):179–193.
7. Trapnell C, Pachter L, Salzberg SL (2009) TopHat: Discovering splice junctions with RNA-Seq. *Bioinformatics* 25(9):1105–1111.
8. Trapnell C, et al. (2010) Transcript assembly and quantification by RNA-Seq reveals unannotated transcripts and isoform switching during cell differentiation. *Nat Biotechnol* 28(5):511–515.
9. Dweep H, Sticht C, Pandey P, Gretz N (2011) miRWalk–database: Prediction of possible miRNA binding sites by "walking" the genes of three genomes. *J Biomed Inform* 44(5):839–847.

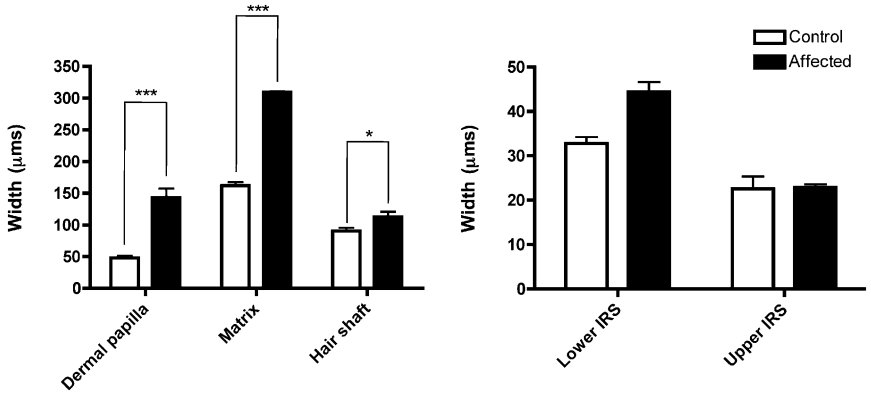

Fig. S1. Morphometric analysis of patient hair follicles reveals matrix, dermal papilla, and hair shaft defects. Quantification of hair follicle components using the length-measuring tool in the AxioVision program revealed a widened dermal papilla (threefold increase; $P = 0.0000343$), matrix (1.9-fold increase; $P = 0.0000642$), and hair shaft (1.25-fold increase; $P = 0.036$). Inner root sheath (IRS) differences in the lower and upper outer root sheath were not statistically significant. Hair follicles were analyzed from one control and two affected individuals, where the average widest distance was calculated for each hair follicle structure. A Student *t* test was performed comparing the affected to the control value with a cutoff *P* value of 0.05 for statistical significance; $*P < 0.05$; $***P < 0.001$. Error bars represent the SD.

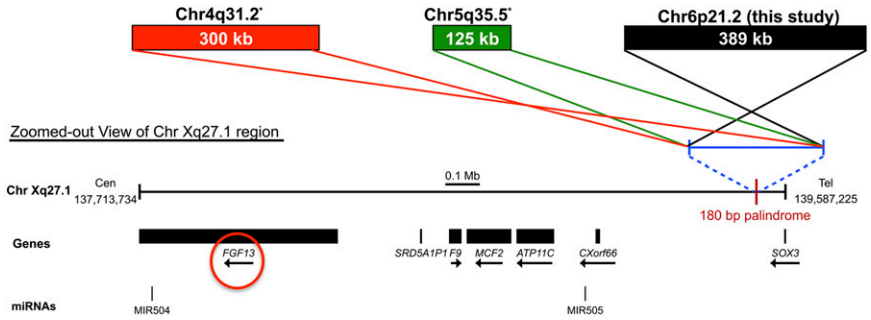

Fig. S2. Summary of interchromosomal insertion events in all three X-linked congenital generalized hypertrichosis families. Zoomed-out view of chromosome Xq27.1 region in X-linked hypertrichosis, where boxes indicate the insertion events and sizes of each from chromosomes 4, 5, and 6. Colored lines connected to the inverted triangle indicate orientation of the insertion events, where all three occur at the same palindromic sequence at Xq27.1. *, corresponds to ref. 1.

1. Zhu H, et al. (2011) X-linked congenital hypertrichosis syndrome is associated with interchromosomal insertions mediated by a human-specific palindrome near SOX3. *Am J Hum Genet* 88(6):819–826.

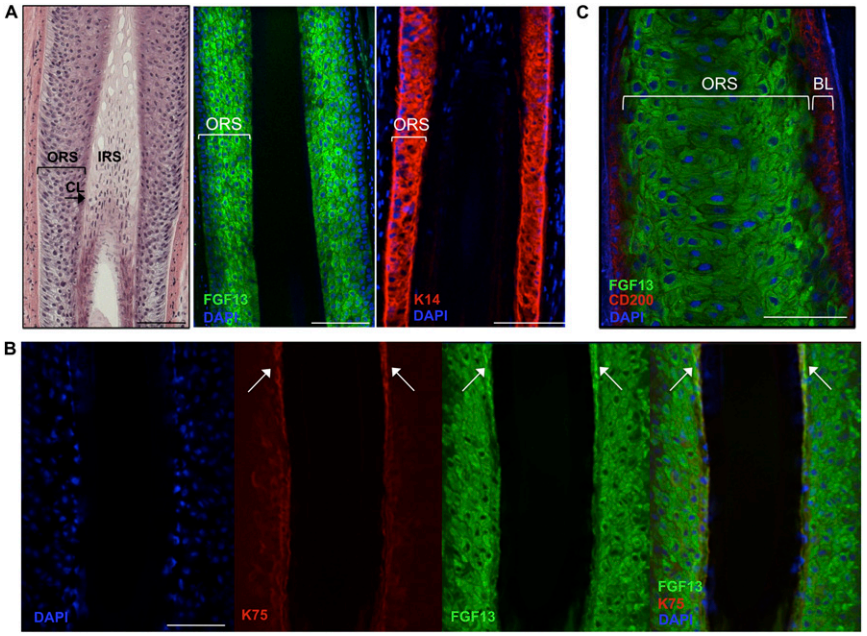

Fig. S3. FGF13 localizes to all layers of the outer root sheath (ORS) and the companion layer but not the human hair follicle bulge. (*A*) Immunofluorescence staining of FGF13 juxtaposed with Keratin 14 (KRT14) (which marks all layers of the ORS) demonstrates that FGF13 is broadly expressed throughout the ORS. The far right image is a hematoxylin-and-eosin staining of an anagen hair follicle for reference of morphology. (*B*) Costaining of FGF13 with KRT75, a marker of the companion layer between the ORS and inner root sheath (IRS), demonstrates that FGF13 localizes to the companion layer (arrows). (*C*) Costaining of FGF13 and CD200 (a marker of the bulge region of the hair follicle) demonstrates that FGF13 does not localize to the human hair follicle bulge. BL, basal layer. (Scale bar, 100 μm.)

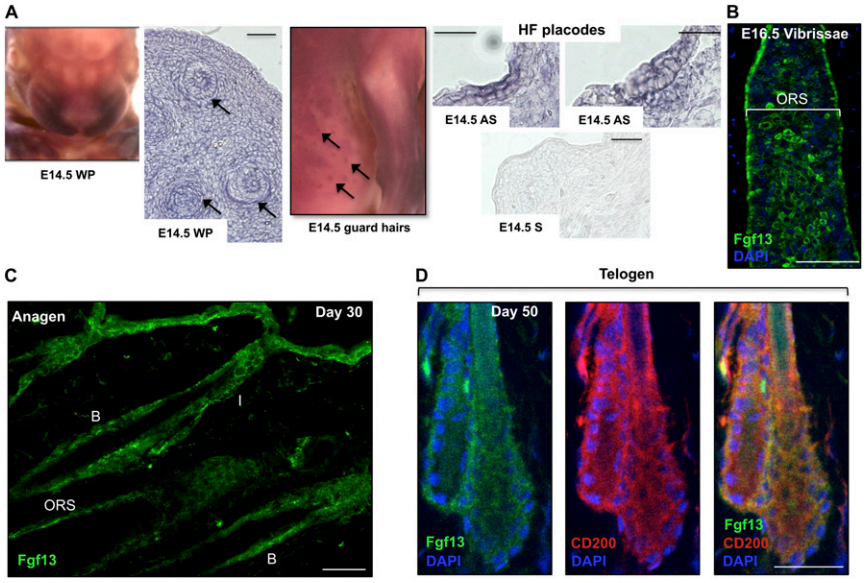

Fig. S4. *Fgf13* is expressed in the developing and cycling mouse hair follicle. (*A*) Whole-mount and section in situ hybridization of *Fgf13* on embryonic day 14.5 (E14.5) embryos reveals expression in the developing whisker pad (WP), guard hair follicle placodes, and dermal condensates at E14.5 ($n = 3$; AS, antisense; S, sense). Arrows indicate vibrissa and guard hair follicles. (*B*) Immunofluorescence staining on E16.5 vibrissae follicles demonstrates that Fgf13 localizes to the outer root sheath (ORS) ($n = 3$). (*C*) Immunofluorescence staining of Fgf13 in anagen (day 30) hair follicles reveals that Fgf13 localizes to the bulge (B), isthmus (I), and ORS. (*D*) Costaining of Fgf13 and CD200 in telogen (day 50) hair follicles reveals that Fgf13 localizes to the bulge. (Scale bar, 100 μm.)

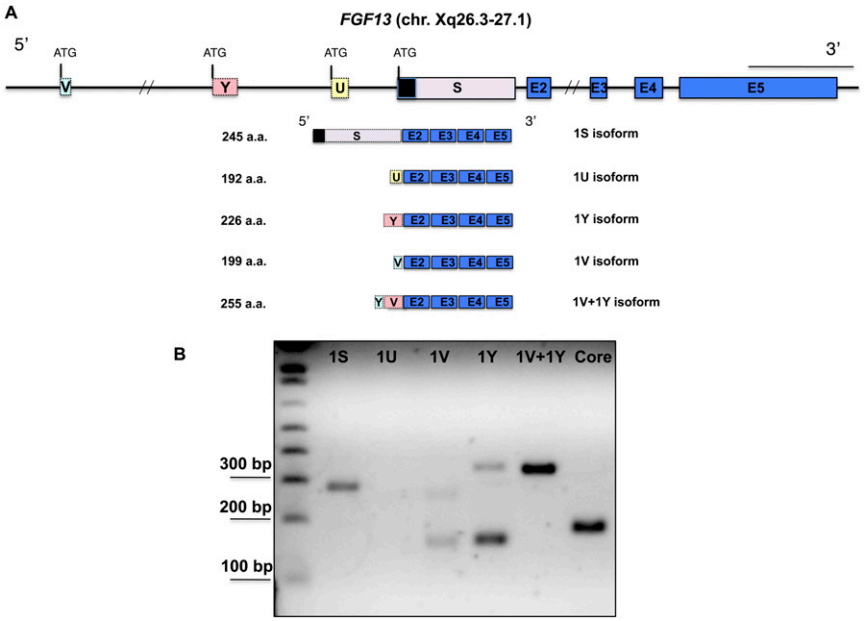

Fig. S5. Isoform-specific PCR of *FGF13* in whole skin. (*A*) Schematic of the *FGF13* locus at chromosome Xq26.3–27.1 (chr. Xq26.3–27.1). Alternating 5′ exons (termed 1S, 1U, 1V, 1Y, and 1V+1Y) are represented as boxes with distinct colors, whereas exons 2–5, common to all transcripts, are shown as blue boxes. The dark box at the 5′ end of the 1S isoform represents a nuclear localization signal. (Scale bar at top right, 100 kb.) (*B*) Amplification of *FGF13* transcripts using cDNA from whole skin demonstrates that the 1S, 1Y, and 1V+1Y isoforms are strongly expressed, and the V isoform is faintly expressed. "Core" represents the 3′ region common to all these isoforms. The Ensembl transcripts corresponding to these splice variants are *FGF13-001* (1S), *FGF13-002* (1U), *FGF13-203* (1V), *FGF13-202* (1Y), and *FGF13-201, -3* (1V+Y).

Table S1. X chromosome inactivation experiment in XLH female carriers

Sample ID	Description	% skewing
II-2	Female carrier	43
II-9	Female carrier	81
II-1	Female carrier	67
II-6	Female carrier	62
III-11	Female carrier	74
II-8	Female nonaffected	Noninformative
III-8	Female nonaffected	Noninformative

Table S2. Differential expression of FGF13 (bolded) and other genes ~3 Mb on either side of the 389-kb insertion (underlined and italicized) at Xq27.1 by RNA-seq

Gene name	Locus	Detectable expression	ln(fold change affected vs. unaffected)	Fold change (affected vs. unaffected)	*P* value
ZIC3	Chr:136476011–136481925	No	N.D.	N.D.	0.213
LOC158696	Chr:137524557–137527465	No	N.D.	N.D.	0.159
FGF13	**Chr:137541399–138114851**	**Yes**	**2.076**	**−7.976**	**0.012**
MIR504	Chr:137541399–138114851	No	N.D.	N.D.	1.000
LOC100129662	Chr:137541399–138114851	No	N.D.	N.D.	1.87*E*-05
Pseudogene (SRD5A1P1)	Chr:138356643–138358798	Yes	1.562	−4.770	0.005
F9	Chr:138440560–138473283	No	N.D.	N.D.	0.023
MCF2	Chr:138491595–138618047	Yes	0.320	−1.376	0.501
ATP11C	Chr:138636170–138742113	Yes	0.184	−1.201	0.663
MIR505	Chr:138833972–138834056	No	N.D.	N.D.	1.000
CXorf66	Chr:138865549–138875343	No	N.D.	N.D.	1.000
Insertion at chrX:139,330,620					
SOX3	Chr:139412817–139414891	No	N.D.	N.D.	1.000
RP1-177G6.2	Chr:139619589–139624662	No	N.D.	N.D.	0.677
CDR1	Chr:139693090–139694389	Yes	0.567	−1.763	0.387
MIR320D2	Chr:139836002–139836050	No	N.D.	N.D.	1.000
SPANXB1	Chr:139924426–139925542	No	N.D.	N.D.	1.000
LDOC1	Chr:140097596–140098976	Yes	0.382	−1.465	0.484
SPANXC	Chr:140163261–140164312	No	N.D.	N.D.	1.000
SPANXA1	Chr:140418508–140565735	No	N.D.	N.D.	1.000
SPANXA2	Chr:140418508–140565735	No	N.D.	N.D.	1.000
SPANXA2-OT1	Chr:140418508–140565735	No	N.D.	N.D.	0.079
SPANXD	Chr:140613233–140614321	No	N.D.	N.D.	1.000
SPANXE	Chr:140613233–140614321	No	N.D.	N.D.	1.000
MAGEC3	Chr:140753767–140813284	No	N.D.	N.D.	0.159
MAGEC1	Chr:140819307–140824853	No	N.D.	N.D.	1.000
MAGEC2	Chr:141117793–141120742	No	N.D.	N.D.	1.000
SPANXN4	Chr:141941369–141949732	No	N.D.	N.D.	1.000

Genomic coordinates reference UCSC Genome Browser human reference hg18. ln, natural logarithm; N.D., not detectable.

Table S3. miR-504 predicted target genes differentially expressed in XLH by RNA-seq

Gene name	Locus	Fold change (affected vs. unaffected)	ln(fold change)	*P* value	*Q* value
BATF2	Chr11:64511992–64521093	40.711	−3.707	0.001	0.008
FZD9	Chr7:72486044–72488386	34.025	−3.527	1.80*E*-05	0.000
TGM4	Chr3:44891101–44931092	31.450	−3.448	0.002	0.015
NPTX1	Chr17:76055227–76064999	30.048	−3.403	3.92*E*-09	2.91*E*-07
CRTAM	Chr11:122214464–122248557	26.236	−3.267	0.003	0.022
HTR7	Chr10:92490555–92607651	22.499	−3.113	0.000	0.002
UBASH3B	Chr11:122031607–122190397	21.982	−3.090	2.47*E*-08	1.49*E*-06
FUT5	Chr19:5816836–5821551	19.225	−2.956	2.66*E*-05	0.001
ATP8B3	Chr19:1733073–1763270	18.705	−2.929	2.83*E*-08	1.67*E*-06
MDGA1	Chr6:37708261–37773744	16.793	−2.821	6.99*E*-07	2.79*E*-05
FJX1	Chr11:35596310–35598997	11.675	−2.457	5.67*E*-06	0.000
KIF21B	Chr1:199205136–199259451	11.648	−2.455	6.60*E*-13	9.76*E*-11
MET	Chr7:116099694–116225676	10.666	−2.367	1.44*E*-06	5.17*E*-05
TP53RK	Chr20:44619868–44751683	10.417	−2.343	4.26*E*-05	0.001
MALL	Chr2:110198735–110231432	10.377	−2.340	1.09*E*-05	0.000
IL6R	Chr1:152644292–152708550	10.361	−2.338	1.09*E*-08	7.38*E*-07
STC1	Chr8:23755378–23768265	10.269	−2.329	1.39*E*-05	0.000
HAS3	Chr16:67696967–67723994	9.828	−2.285	1.78*E*-08	1.13*E*-06
S100A7A	Chr1:151655623–151662325	8.701	−2.163	3.66*E*-05	0.001
MTHFD2	Chr2:74279197–74295932	8.430	−2.132	2.00*E*-06	6.96*E*-05
CDCP1	Chr3:45098772–45162918	8.277	−2.113	5.62*E*-05	0.001
EXOSC6	Chr16:68841634–68843334	8.037	−2.084	0.000	0.002
TNFRSF9	Chr1:7898517–7925812	8.020	−2.082	0.004	0.030
P2RY11	Chr19:10077898–10091599	7.800	−2.054	0.000	0.002
LPCAT1	Chr5:1514541–1577076	7.264	−1.983	0.000	0.003

Table S3. Cont.

Gene name	Locus	Fold change (affected vs. unaffected)	ln(fold change)	*P* value	*Q* value
LIF	Chr22:28966441–28972796	6.932	−1.936	0.000	0.003
PNO1	Chr2:68238508–68256595	6.650	−1.895	0.000	0.005
BYSL	Chr6:41996942–42008762	5.907	−1.776	0.001	0.009
TRIB3	Chr20:309307–326203	5.706	−1.742	0.001	0.010
PCDH10	Chr4:134289919–134332182	5.591	−1.721	0.005	0.033
BCAT1	Chr12:24854224–24993660	5.357	−1.678	0.001	0.010
CNO	Chr4:6768742–6770288	5.247	−1.658	0.003	0.023
CYGB	Chr17:72035024–72053053	5.226	−1.654	0.005	0.035
ZFAT	Chr8:135559212–135794474	5.216	−1.652	8.57*E*-08	4.52*E*-06
STK40	Chr1:36577811–36624072	5.210	−1.651	0.002	0.016
SPRED2	Chr2:65391488–65513160	5.123	−1.634	9.36*E*-05	0.002
FUT2	Chr19:53891039–53901003	5.119	−1.633	0.000	0.005
IPPK	Chr9:94099460–94472368	5.105	−1.630	0.002	0.015
PXN	Chr12:119123476–119187957	5.053	−1.620	5.16*E*-08	2.90*E*-06
CD86	Chr3:123256898–123322678	5.052	−1.620	0.001	0.007
ABL2	Chr1:177335084–177465442	5.027	−1.615	9.74*E*-13	1.43*E*-10
KLHL21	Chr1:6573370–6585516	4.985	−1.606	0.007	0.044
FSCN1	Chr7:5598961–5612813	4.963	−1.602	0.004	0.031
RUNX1	Chr21:35081967–35343465	4.835	−1.576	2.14*E*-05	0.001
RRAGC	Chr1:39077605–39097927	4.730	−1.554	0.002	0.020
SERTAD1	Chr19:45620248–45623772	4.697	−1.547	0.003	0.022
OSBP2	Chr22:29420792–29633811	4.695	−1.547	0.005	0.033
ZNF264	Chr19:62394679–62426026	4.653	−1.538	0.004	0.028
DNMBP	Chr10:101625323–101759666	4.581	−1.522	0.003	0.023
PLEKHM1	Chr17:40869048–40923929	4.558	−1.517	2.80*E*-05	0.001
PDRG1	Chr20:29996418–30003544	4.414	−1.485	0.007	0.042
MBP	Chr18:72819776–72973762	4.300	−1.459	3.75*E*-05	0.001
PLCD3	Chr17:40544533–40565417	4.266	−1.451	0.005	0.033
SLC7A1	Chr13:28981550–29067825	4.162	−1.426	0.007	0.043
GMEB2	Chr20:61689398–61728825	4.160	−1.425	0.007	0.041
LRRC8A	Chr9:130684211–130720138	4.158	−1.425	0.000	0.006
KCNK1	Chr1:231816372–231874881	4.037	−1.396	0.006	0.039
NUDT15	Chr13:47509703–47519283	4.004	−1.387	0.008	0.046
LY6K	Chr8:143778530–143805393	3.958	−1.376	0.001	0.006
SMURF1	Chr7:98462993–98579679	3.939	−1.371	0.002	0.016
GPER	Chr7:1003148–1144419	3.871	−1.354	0.008	0.047
RRAS2	Chr11:14256041–14342628	3.637	−1.291	0.000	0.002
CRTC3	Chr15:88874201–88989581	3.559	−1.270	0.001	0.010
MAPKAPK2	Chr1:204924987–204974253	3.464	−1.242	0.005	0.035
ZBTB24	Chr6:109890411–109911133	3.342	−1.207	0.008	0.047
NRF1	Chr7:129038790–129184158	3.334	−1.204	0.006	0.038
DIAPH1	Chr5:140874771–140978806	3.312	−1.197	0.001	0.011
PAPD5	Chr16:48744329–48826720	3.160	−1.151	0.008	0.045
DHX33	Chr17:5284955–5313104	3.083	−1.126	0.003	0.022
PVR	Chr19:49838937–49861268	2.872	−1.055	0.001	0.009
TGFBR1	Chr9:100907232–100956294	2.854	−1.049	0.008	0.046
GAS7	Chr17:9754650–10042593	2.703	−0.994	0.006	0.036
IL1RAP	Chr3:191714533–191857680	2.632	−0.968	0.002	0.015
CTDP1	Chr18:75540788–75615498	2.594	−0.953	0.007	0.044
VEGFA	Chr6:43845923–43862201	2.490	−0.912	0.000	0.005
CNOT4	Chr7:134697086–134845415	2.220	−0.798	0.004	0.026

Genomic coordinates reference UCSC Genome Browser human reference hg18. ln, natural logarithm.

Table S4. FGFs with dysregulated expression levels in XLH by RNA-seq in whole skin

Gene name	Locus	Fold change (patient vs. control)	*P* value
FGF5	Chr4:81406765–81431195	−56.33	2.53*E*-09
FGF18	Chr5:170779271–170817235	−11.22	3.00*E*-05
FGF14	Chr13:101171205–101852125	−9.13	0.0004
FGF13	Chr:137541399–138114851	−7.98	0.012
FGF12	Chr3:193339875–193928082	−6.09	0.006
FGFR1OP	Chr6:167332805–167374056	−3.37	0.007
FGFR3	Chr4:1764836–1780397	−3.21	0.001
FGFR2	Chr10:123227833–123347962	−2.32	0.0008
FGFBP1	Chr4:15546289–15549461	13.58	3.70*E*-06

Genomic coordinates reference UCSC Genome Browser human reference hg18.